



Semnan University

Mechanics of Advanced Composite Structures

journal homepage: <http://MACS.journals.semnan.ac.ir>

Finite Difference Analysis of 2D Stress Wave Propagation in Two Dimensional Functionally Graded Ceramics-Metals Composites

A.R. Amiri, H. Rahmani*

Department of Mechanical Engineering, University of Sistan and Baluchestan, Zahedan, Iran

KEYWORDS

Stress wave propagation
Finite difference
FGM
Ceramic-metal composite

ABSTRACT

In this study, a finite difference method is presented for longitudinal stress wave propagation analysis in functionally graded 2D plane strain media. The plane material consists of two ceramics (SiC and Al_2O_3) and two metals (Al 1100 and Ti-6Al-4V (TC4)) with power-law variation for mechanical properties in terms of volume fractions of the constituents. Firstly, the governing equations of wave propagation in the functionally graded plane strain media were derived in Cartesian coordinate. It's assumed that elastic module, density, and Poisson's ratio are variable in all of the media. Secondly, the finite difference method was used to discretize the equations. Time step size was obtained using the von Neumann stability approach. The materials distribution effects are studied in different states and history of stress, strain, and displacement. To validate the numerical simulation, stress is compared with theoretical equations in special states. Results show that the wave propagation behavior is considerably influenced by material composition variation.

1. Introduction

Functionally graded materials (FGM) were introduced as a new type of composites by Japanese scientists in 1984. These new materials are inhomogeneous in microscopic space and usually consist of ceramic and metal. FGMs were initially used only in spacecraft and nuclear reactors [1] but are now used in military, nuclear, motorized, and aerospace industries where the impact loading effects are important [2-5]. When a media is subjected to impact loading, because of the inertial effects, stress waves propagate on it. The movement of pulse shape waves affects the velocity, displacement, and stress of material particles. The type of stress is depended on the loading condition and can be longitudinal (compression or tensile) or torsional (shear). When the stress wave reaches the diverse discontinuity in media such as section area, elastic module, density, or impedance change, it shows different behaviors. Since the propagation of stress waves is dependent on the impedance of material, the wave motion is influenced by mechanical property changes in FGMs. Many studies have been done concerning one or two dimensional wave propagation in FGMs [6-10]. In

these researches, the elastodynamic behavior of the considered structure was analyzed from different aspects by dividing the waves into a bulk wave, plane wave or surface wave, harmonic or transient wave, in Cartesian or polar coordinate, etc. The 2D wave propagation in an elastic isotropic semi-infinite cylindrical rod that is subjected to normal impulsive load was studied by Alterman and Karal [11]. The equations were solved using the finite difference method in polar coordinates in the z and r directions. Chiu and Erdogan [12] investigated the one dimensional stress wave propagation in a functionally graded elastic slab. The slab was made of nickel/zirconia or aluminum/silicon. They assumed that the stiffness and density of the medium vary continuously in the thickness direction and initially, it is at rest and stress-free conditions. They also reported the distortion, peak stress, and energy balance. Bruck [13] optimized the failure resistance of the FGMs in order to use them as energy absorbers. For this aim, they proposed a one-dimensional model to develop the stress wave management issues. The proposed model was initially applied to discrete layer FGMs with continuously graded architectures. Han et al. [14] used a numerical

* Corresponding author. Tel.: +98-54-31132378 ; Fax: +98-54-33447092
E-mail address: H_Rahmani@eng.usb.ac.ir

method to analyze the effect of transient waves in cylindrical shells of a functionally graded material (FGM) subjected to impact point load. The material property within each element was assumed to vary linearly in the thickness direction and as a result, the displacement response of FGM shells excited by point loads was calculated, and the characteristics of waves in FGM shells were discussed. The elastic wave propagation in a layered media was investigated using a finite difference method by Tadi [15]. They presented two finite difference formulations for elastic wave propagation. Both of them had explicit scheme and were of the second order accuracy in time and space. Asemi et al. [16] considered a thick short length hollow cylinder made of functionally graded materials (FGMs) under internal impact loading. They used a finite element method based on Rayleigh-Ritz energy to study the propagation of elastic waves. Stress, displacement, wave propagation, and natural frequency of the hollow wall were also reported.

The propagation of surface waves such as Love waves [17], Lamb waves [18, 19], and SH-wave [20] in FG materials and Rayleigh wave motions in an orthotropic half-space under time harmonic loadings [21] have also been studied. The Simultaneous effects of Nonlinear transient thermal stress and elastic wave propagation analysis in hollow thick temperature-dependent FGM cylinders, using a second-order point-collocation method was investigated by Shariyat et.al [22]. In a similar research, an exact elastodynamic solution for functionally graded thick-walled cylinders subjected to dynamic pressures was investigated in [23]. In another research, Hosseini and Abolbashar found a general analytical solution for elastic radial wave propagation and dynamic analysis of functionally graded thick hollow cylinders subjected to impact loading [24]. Wave propagation in functionally graded and layered materials was analyzed using the space-time discontinuous Galerkin method in [25]. Using the finite-difference method the elastic wave propagation in functionally graded circular cylinders [26] and disks [27] have been investigated. In both of these papers, the impulsive load is assumed to be applied in the axial direction and then the stress and displacement fields were calculated.

To address recent contributions, the Optimization of volume fraction distribution in a thick hollow heterogeneous was studied by Asgari [28]. The considered cylinder was subjected to impulsive internal pressure. The main objective was to minimize the amplitude of stress waves propagating through the structure during a specified time interval. Bednarik et al. [29] investigated the propagation of one-

dimensional propagation of longitudinal elastic waves through a plate that is made of FGMs with the assumption of material distribution according to trigonometric law. Yang and Liu [30] proposed a new boundary element method for modeling the 2-D wave propagation problem in FGM materials in the frequency domain. They investigated gradation direction and frequency on the wave propagation.

In most of the mentioned researches, the mechanical properties of materials change only in one direction. In the current paper, a two dimensional wave propagation analysis in a plane strain media is performed. The media consists of two elastic metals (SiC and Al_2O_3) and two elastic ceramics (Al 1100 and Ti-6Al-4V) with power law variation of mechanical properties in terms of volume fractions of the constituents for both of the x and y directions. Two impulsive loadings are applied to this media and consequently, elastic waves propagate on it. The governing equations of the wave motion in assumed media are achieved by elastodynamic theories. A finite difference scheme is used to solve the governing equations. Later on, displacement, stress, and strain fields are calculated. The positions of pure materials in different corners are changed and the effect of material distribution will be investigated too. The verification of the proposed model is achieved through comparison with existing published results. The main contributions of this paper are summarized as follows.

Firstly, in most of the researches, the wave is considered to be harmonic. By this consideration, wave propagation equations can be solved by the separation of variables. While in the present study, the transient response of media under impact loading is investigated.

Secondly, considering the FGM structure as a two dimensional media that the material properties are changed in x and y directions while in other researches materials properties vary only in one direction, and also in the presented study, the stress wave is propagated in two directions.

Thirdly, all of the mechanical properties such as density, elastic module, and Poisson's ratio are assumed to be variable, while in most studies, the Poisson's ratio is considered constant.

Moreover, the loading of the media is applied in x and y directions.

On the other hand, the history of researches shows that in all studies, FGMs are made of only two materials while in some applications it's needed to use a combination of materials with different mechanical and thermal properties. For example, nowadays, FGM turbine blades are made of ceramic-metal composite. The external parts are made of ceramic because of its good

thermal and mechanical properties and their strength against the impact loading of floating particles. The internal parts are made of metal due to their good heat transfer properties.

It is noteworthy that in an FGM blade, the stress on the root of the blade is more than the tip because of the moment. While heat transfer and thermal properties are more important in the tip of the blade. Moreover, the lower density of the blade tip can reduce the centrifuge stresses. So that, apart from the fact that we need the material changes in thickness, sometimes it's better to change the properties in other directions.

In summary, this study presents a generalized and extended solution for stress wave propagation in FGM's rather than the previous researches that results of it can be potentially used for designing the energy absorbers.

2. Problem formulation

2.1. Material properties definition for 2D functionally graded media

2D functionally graded materials (2D-FGM) are made by several continuous gradient phases. In the present research, the material distribution is selected based on the volume fraction in the 2D-FGM cylinder reported by Asgari and Akhlaghi [31] and generalizing it to a cartesian coordinate. To this aim, a Cartesian coordinate is defined to contain the reference point in (0, 0) and x and y-axis. The length of sides in x and y directions are L_x and L_y respectively, as shown in Fig. 1. To satisfy the plane strain condition, the depth (z-direction) of Fig. 1 is considered to be infinite.

The volume fraction of each material in functionally graded media is reported in Eqs. 1a to 1d.

$$V_{c1} = \left(1 - \left(\frac{x}{b}\right)^{n_x}\right) \left(\frac{y}{b}\right)^{n_y} \tag{1a}$$

$$V_{c2} = \left(1 - \left(\frac{x}{b}\right)^{n_x}\right) \left(1 - \left(\frac{y}{b}\right)^{n_y}\right) \tag{1b}$$

$$V_{m1} = \left(\frac{x}{b}\right)^{n_x} \left(\frac{y}{b}\right)^{n_y} \tag{1c}$$

$$V_{m2} = \left(\frac{x}{b}\right)^{n_x} \left(1 - \left(\frac{y}{b}\right)^{n_y}\right) \tag{1d}$$

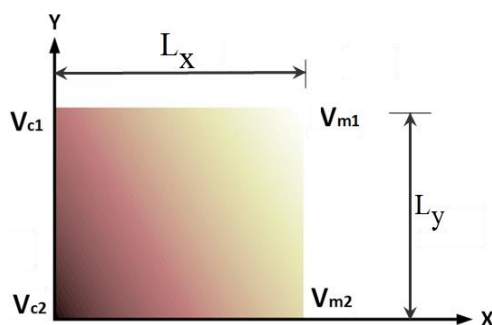


Fig. 1. Cartesian coordinate with 2D material distribution

where n_x and n_y represent the constituent distributions in x and y directions and subscripts m and C denote metal and ceramic phases.

To use volume fractions, the following rules in Eq. (2) should be considered:

$$\begin{aligned} V_{c1} + V_{c2} + V_{m1} + V_{m2} &= 1 \\ 0 \leq V_{c1} &\leq 1 \\ 0 \leq V_{c2} &\leq 1 \\ 0 \leq V_{m1} &\leq 1 \\ 0 \leq V_{m2} &\leq 1 \end{aligned} \tag{2}$$

Material properties at each point can be obtained by using the linear rule of mixtures. Material property, P (P could be an elastic module, density and Poisson's ratio) at any arbitrary point (x, y) in the 2D-FGM media is determined by a linear combination of volume fractions and material properties of the basic materials, from Eq. (3).

$$P = P_{c1}V_{c1} + P_{c2}V_{c2} + P_{m1}V_{m1} + P_{m2}V_{m2} \tag{3}$$

where P_{c1} , P_{c2} , P_{m1} , P_{m2} are properties of pure materials.

2.2. Governing Equations

The Cartesian coordinate system (x, y, z) is assumed to simulate the stress wave propagation in 2D FGM. Due to the plane strain condition, the deformation is considered to be negligible in the z-direction. So for 2D media in the absence of the body forces, equations of motion in terms of stress component are given by Eq. (4) [32]

$$\begin{aligned} \frac{\partial \sigma_{xx}}{\partial x} + \frac{\partial \sigma_{xy}}{\partial y} &= \rho \frac{\partial^2 u}{\partial t^2} \\ \frac{\partial \sigma_{xy}}{\partial x} + \frac{\partial \sigma_{yy}}{\partial y} &= \rho \frac{\partial^2 v}{\partial t^2} \end{aligned} \tag{4}$$

where $u(x, y)$ and $v(x, y)$ are the displacement components, σ_{xx} and σ_{yy} are normal stresses in x and y directions respectively. σ_{xy} is the shear stress component, t is time and ρ is the density.

The constitutive equations of the functionally graded media can be expressed as Eq. 5. [33]

$$\begin{aligned} \sigma_{xx} &= (\lambda + 2\mu) \frac{\partial u}{\partial x} + \lambda \frac{\partial v}{\partial y} \\ \sigma_{yy} &= (\lambda + 2\mu) \frac{\partial v}{\partial y} + \lambda \frac{\partial u}{\partial x} \\ \sigma_{xy} &= \mu \left(\frac{\partial u}{\partial y} + \frac{\partial v}{\partial x} \right) \end{aligned} \tag{5}$$

The properties of the elastic medium are given by the Lamé constants. λ and μ in Eq. (5) can be obtained from Eq. (6).

$$\lambda(x, y) = \frac{E(x, y)\nu(x, y)}{(1 + \nu(x, y))(1 - 2\nu(x, y))} \tag{6}$$

$$\mu(x, y) = \frac{E(x, y)}{2(1 + \nu(x, y))}$$

To write the equation of motion in terms of displacements, substituting Eq. (5) in Eq. (4) yields Eq. (7)

$$(\lambda + 2\mu) \frac{\partial^2 u}{\partial x^2} + \mu \frac{\partial^2 u}{\partial y^2} + (\lambda + \mu) \frac{\partial^2 v}{\partial x \partial y} + (\lambda_x + 2\mu_x) \frac{\partial u}{\partial x} + \mu_y \frac{\partial u}{\partial y} + \lambda_x \frac{\partial v}{\partial y} + \tag{7a}$$

$$\mu_y \frac{\partial v}{\partial x} = \rho \frac{\partial^2 u}{\partial t^2}$$

$$(\lambda + 2\mu) \frac{\partial^2 v}{\partial y^2} + \mu \frac{\partial^2 v}{\partial x^2} + (\lambda + \mu) \frac{\partial^2 u}{\partial x \partial y} + (\lambda_y + 2\mu_y) \frac{\partial v}{\partial y} + \mu_x \frac{\partial v}{\partial x} + \lambda_y \frac{\partial u}{\partial x} + \tag{7b}$$

$$\mu_x \frac{\partial u}{\partial y} = \rho \frac{\partial^2 u}{\partial t^2}$$

By solving these equations, displacement fields are calculated, using the resultant relations one can obtain the stress and strain distribution in different x and y.

2.3. Initial and Boundary condition

As mentioned before, the 2D FGM media is composed of four materials containing two metals (Ti-6Al-4V and Al 1100) and two ceramics (SiC and Al₂O₃). The mechanical properties of these materials are shown in Table 1.

Table 1. Mechanical properties of 2D FGM media [34].

Constituents	Material	E (GPa)	ρ (kg/m ³)	ν
m1	Ti-6Al-4V	115	4515	0.31
m2	Al 1100	69	2715	0.33
C1	SiC	440	3210	0.14
C2	Al ₂ O ₃	150	3470	0.21

The dimensions of the plane strain body are considered to be 1 m in the x-direction (L_x) and 0.5 m in the y-direction (L_y).

To investigate the effect of compositional gradient exponents (n_x, n_y), 5 states are assumed. As shown in Fig.1, there are two materials in top of the surface (C₁ and m₁), two materials in bottom surface (C₂ and m₂), two materials in right hand surface (m₁ and m₂), and two materials in left hand side (C₁ and C₂). For different n_x and n_y, the richness of each of the materials changes is shown in Table 2.

It's to be mentioned that if L_x = L_y, the volume fraction of material in some states are equal.

The gradient of the elastic module, density, and Poisson's ratio in the first state are shown in Fig 2.

As can be seen, unlike composites that their properties change stepwise, in the FG materials, the properties are changed uniformly. This unique feature of these materials, which was described in the previous sections, has led to more applications.

Table 2. Compositional gradient exponents (n_x, n_y) and the materials distribution.

	N _x	n _y	Volume fraction compression
State 1	1	1	V _{m1} = V _{m2} = V _{C1} = V _{C2}
State 2	0.2	0.2	V _{m1} > V _{m2} > V _{C1} > V _{C2}
State 3	5	5	V _{m1} < V _{m2} < V _{C1} < V _{C2}
State 4	0.2	5	V _{m2} > V _{m1} > V _{C2} > V _{C1}
State 5	5	0.2	V _{m2} < V _{m1} < V _{C2} < V _{C1}

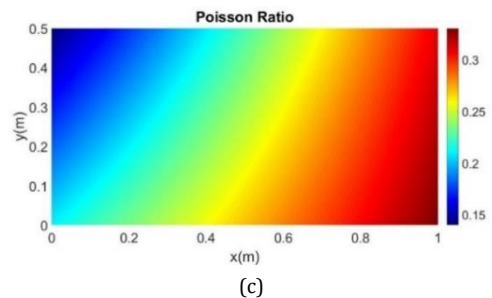
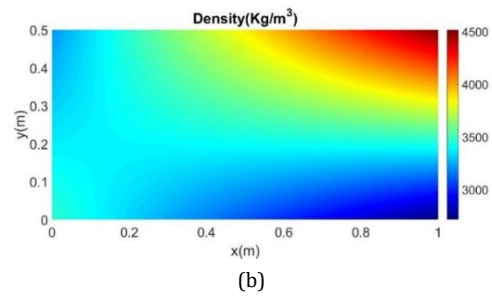
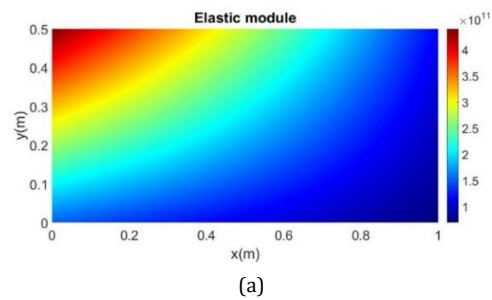


Fig. 2. The gradient of elastic module (a), density (b), and Poisson's ratio (c) in the first state

In this research, it has been considered that two impact loads are applied on the x and y directions. The surfaces are free. The time variation of impact loads is assumed as the following function in Eq. (8).

$$F = P \cdot \omega(t) \tag{8}$$

where P = 106 Pa. Variation of the loading P. ω(t) was represented by ramped loading and unloading paths as shown in Fig 3. The loading is started in time t = 0 and in t = 10 μs it reaches the maximum value which is equal to 1 MPa and then it starts to unloading and finally in t = 20 μs the load value reduces to zero.

Initial conditions are indicated at t= 0 as follows:

$$\frac{\partial u}{\partial t} = \frac{\partial v}{\partial t} = 0 \quad \text{and} \quad u = v = 0 \tag{9}$$

This means that the displacement and velocity of the particles in t = 0 are equal to zero. In addition, lateral boundaries in the top and right hand edges of Fig. 4 are assumed to be free. The traction boundary conditions are also taken into account for this problem. The compressive force input to the functionally graded media is always entered at the x = 0 and y = 0 axes (the bottom and left hand edges in Fig. 4).

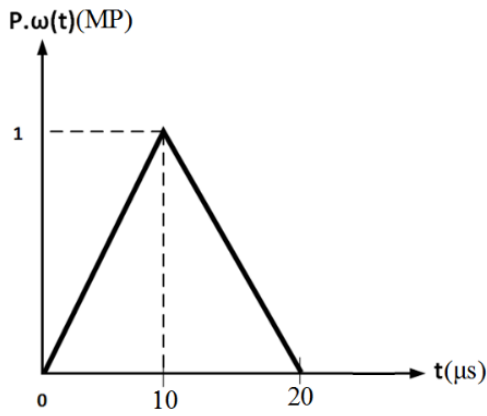


Fig. 3. Time variation of loading and unloading.

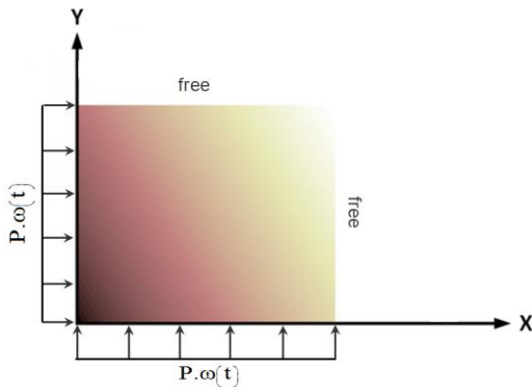


Fig. 4. The boundary condition of the problem.

2.4. Finite-difference implementation

The finite difference is one of the well-known methods for solving differential equations. This method consists of approximating the differential operator by replacing the derivatives in the equation using differential quotients. In this article, for both spatial and temporal derivatives, central difference approximations have been used. The grid size is uniform in both directions. Let Δx and Δy be the grid sizes and N_x and N_y be the total mesh points in the x and y direction respectively [35]. In this study, Δx and Δy are equal to 0.01 m, N_x and N_y are taken to be 100 and 50 respectively. According to this, 5000 elements exist in the final model.

By substituting centered difference equations of the second order derivatives of a displacement component with respect to the time t and spatial variables x and y at the nodal point (i, j) in Eq. (7) we obtain:

$$\begin{aligned} & (\lambda_{i,j} + 2\mu_{i,j}) \left(\frac{u_{i+1,j}^k - 2u_{i,j}^k + u_{i-1,j}^k}{(\Delta x)^2} \right) + \\ & \mu_{i,j} \left(\frac{u_{i,j+1}^k - 2u_{i,j}^k + u_{i,j-1}^k}{(\Delta y)^2} \right) + \\ & (\lambda_{i,j} + \mu_{i,j}) \times \\ & \left(\frac{v_{i+1,j+1}^k - v_{i-1,j+1}^k + v_{i-1,j-1}^k - v_{i+1,j-1}^k}{4\Delta x \Delta y} \right) \\ & + \left(\frac{\lambda_{i+1} - \lambda_{i-1}}{2\Delta x} + 2 \frac{\mu_{i+1} - \mu_{i-1}}{2\Delta x} \right) \times \\ & \left(\frac{u_{i+1} - u_{i-1}}{2\Delta x} \right) + \left(\frac{\mu_{j+1} - \mu_{j-1}}{2\Delta y} \right) \times \\ & \left(\frac{u_{j+1} - u_{j-1}}{2\Delta y} + \frac{v_{i+1} - v_{i-1}}{2\Delta x} \right) \\ & + \left(\frac{\lambda_{i+1} - \lambda_{i-1}}{2\Delta x} \right) \left(\frac{v_{j+1} - v_{j-1}}{2\Delta y} \right) = \\ & \rho_{i,j} \left(\frac{u_{i,j}^{k+1} - 2u_{i,j}^k + u_{i,j}^{k-1}}{(\Delta t)^2} \right) \\ & (\lambda_{i,j} + 2\mu_{i,j}) \left(\frac{v_{i+1,j}^k - 2v_{i,j}^k + v_{i-1,j}^k}{(\Delta y)^2} \right) \\ & + \mu_{i,j} \left(\frac{v_{i,j+1}^k - 2v_{i,j}^k + v_{i,j-1}^k}{(\Delta x)^2} \right) \\ & + (\lambda_{i,j} + \mu_{i,j}) \times \\ & \left(\frac{u_{i+1,j+1}^k - u_{i-1,j+1}^k + u_{i-1,j-1}^k - u_{i+1,j-1}^k}{4\Delta x \Delta y} \right) \\ & + \left(\frac{\lambda_{i+1} - \lambda_{i-1}}{2\Delta y} + 2 \frac{\mu_{i+1} - \mu_{i-1}}{2\Delta y} \right) \times \\ & \left(\frac{v_{i+1} - v_{i-1}}{2\Delta y} \right) + \left(\frac{\mu_{j+1} - \mu_{j-1}}{2\Delta x} \right) \times \\ & \left(\frac{v_{j+1} - v_{j-1}}{2\Delta x} + \frac{u_{i+1} - u_{i-1}}{2\Delta y} \right) \\ & + \left(\frac{\lambda_{i+1} - \lambda_{i-1}}{2\Delta y} \right) \left(\frac{u_{j+1} - u_{j-1}}{2\Delta x} \right) = \\ & \rho_{i,j} \left(\frac{v_{i,j}^{k+1} - 2v_{i,j}^k + v_{i,j}^{k-1}}{(\Delta t)^2} \right) \end{aligned} \tag{10a}$$

$$\begin{aligned} & \left(\frac{u_{i+1} - u_{i-1}}{2\Delta x} \right) + \left(\frac{\mu_{j+1} - \mu_{j-1}}{2\Delta y} \right) \times \\ & \left(\frac{u_{j+1} - u_{j-1}}{2\Delta y} + \frac{v_{i+1} - v_{i-1}}{2\Delta x} \right) \\ & + \left(\frac{\lambda_{i+1} - \lambda_{i-1}}{2\Delta x} \right) \left(\frac{v_{j+1} - v_{j-1}}{2\Delta y} \right) = \\ & \rho_{i,j} \left(\frac{u_{i,j}^{k+1} - 2u_{i,j}^k + u_{i,j}^{k-1}}{(\Delta t)^2} \right) \\ & (\lambda_{i,j} + 2\mu_{i,j}) \left(\frac{v_{i+1,j}^k - 2v_{i,j}^k + v_{i-1,j}^k}{(\Delta y)^2} \right) \\ & + \mu_{i,j} \left(\frac{v_{i,j+1}^k - 2v_{i,j}^k + v_{i,j-1}^k}{(\Delta x)^2} \right) \\ & + (\lambda_{i,j} + \mu_{i,j}) \times \\ & \left(\frac{u_{i+1,j+1}^k - u_{i-1,j+1}^k + u_{i-1,j-1}^k - u_{i+1,j-1}^k}{4\Delta x \Delta y} \right) \\ & + \left(\frac{\lambda_{i+1} - \lambda_{i-1}}{2\Delta y} + 2 \frac{\mu_{i+1} - \mu_{i-1}}{2\Delta y} \right) \times \\ & \left(\frac{v_{i+1} - v_{i-1}}{2\Delta y} \right) + \left(\frac{\mu_{j+1} - \mu_{j-1}}{2\Delta x} \right) \times \\ & \left(\frac{v_{j+1} - v_{j-1}}{2\Delta x} + \frac{u_{i+1} - u_{i-1}}{2\Delta y} \right) \\ & + \left(\frac{\lambda_{i+1} - \lambda_{i-1}}{2\Delta y} \right) \left(\frac{u_{j+1} - u_{j-1}}{2\Delta x} \right) = \\ & \rho_{i,j} \left(\frac{v_{i,j}^{k+1} - 2v_{i,j}^k + v_{i,j}^{k-1}}{(\Delta t)^2} \right) \end{aligned} \tag{10b}$$

Now by arranging the Eq. (10) finally we get:

$$u_{i,j}^{k+1} = \frac{(\Delta t)^2}{\rho_{i,j}} \left\{ \begin{aligned} &(\lambda_{i,j} + 2\mu_{i,j}) \left(\frac{u_{i+1,j}^k - 2u_{i,j}^k + u_{i-1,j}^k}{(\Delta x)^2} \right) + \\ &\mu_{i,j} \left(\frac{u_{i,j+1}^k - 2u_{i,j}^k + u_{i,j-1}^k}{(\Delta y)^2} \right) + \\ &(\lambda_{i,j} + \mu_{i,j}) \times \\ &\left(\frac{v_{i+1,j+1}^k - v_{i+1,j}^k + v_{i-1,j+1}^k - v_{i-1,j}^k}{4\Delta x \Delta y} \right) \\ &+ \left(\frac{\lambda_{i+1} - \lambda_{i-1}}{2\Delta x} + 2 \frac{\mu_{i+1} - \mu_{i-1}}{2\Delta x} \right) \times \\ &\left(\frac{u_{i+1} - u_{i-1}}{2\Delta x} \right) + \left(\frac{\mu_{j+1} - \mu_{j-1}}{2\Delta y} \right) \times \\ &\left(\frac{u_{j+1} - u_{j-1}}{2\Delta y} + \frac{v_{i+1} - v_{i-1}}{2\Delta x} \right) \\ &+ \left(\frac{\lambda_{j+1} - \lambda_{j-1}}{2\Delta x} \right) \left(\frac{v_{j+1} - v_{j-1}}{2\Delta y} \right) \\ &+ 2u_{i,j}^k - u_{i,j}^{k-1} \end{aligned} \right. \quad (11a)$$

$$v_{i,j}^{k+1} = \frac{(\Delta t)^2}{\rho_{i,j}} \left\{ \begin{aligned} &(\lambda_{i,j} + 2\mu_{i,j}) \left(\frac{v_{i+1,j}^k - 2v_{i,j}^k + v_{i-1,j}^k}{(\Delta y)^2} \right) \\ &+ \mu_{i,j} \left(\frac{v_{i,j+1}^k - 2v_{i,j}^k + v_{i,j-1}^k}{(\Delta x)^2} \right) \\ &+ (\lambda_{i,j} + \mu_{i,j}) \times \\ &\left(\frac{u_{i+1,j+1}^k - u_{i+1,j}^k + u_{i-1,j+1}^k - u_{i-1,j}^k}{4\Delta x \Delta y} \right) \\ &+ \left(\frac{\lambda_{i+1} - \lambda_{i-1}}{2\Delta y} + 2 \frac{\mu_{j+1} - \mu_{j-1}}{2\Delta y} \right) \times \\ &\left(\frac{v_{j+1} - v_{j-1}}{2\Delta y} \right) \\ &+ \left(\frac{\mu_{i+1} - \mu_{i-1}}{2\Delta x} \right) \left(\frac{v_{i+1} - v_{i-1}}{2\Delta x} + \frac{u_{j+1} - u_{j-1}}{2\Delta y} \right) \\ &+ \left(\frac{\lambda_{j+1} - \lambda_{j-1}}{2\Delta y} \right) \left(\frac{u_{i+1} - u_{i-1}}{2\Delta x} \right) \\ &+ 2v_{i,j}^k - v_{i,j}^{k-1} \end{aligned} \right. \quad (11b)$$

In Eq. (11) Δt is the time step size and k refers to the time index that varies from 0 to n_t , the total number of time steps. In this research, the explicit finite difference method has been used. In the explicit method, the equation is solved for $t + \Delta t$ by using the specified current state of the problem (at time t), the problem state at time t is determined and the stiffness matrix is also known at this moment. the time step size Δt is determined using the von Neumann stability criterion [36].

3. Numerical result

3.1. Validation of numerical results

In order to verify the derived model and solutions, firstly we reduce the governing equations of FGM material to a homogenous material (Ti-6Al-4V) and compare the obtained

results with [7]. If the gradient variation of material properties vanishes, the equations would describe a homogenous material. So, we substitute the Young modulus, density, and Poisson's ratio of Ti-6Al-4V in the equations 10 and 11 as well as considering n_x and n_y equal to zero. Consequently, the material properties are constant at all points. The results have been obtained by writing an appropriate program in MATLAB.

Figure 5 shows the behavior of wave, 35 μs after propagating in media that is made completely from Ti-6Al-4V. As it can be seen, the wave in the x and y directions is moving and in a special point, two waves interfere together that causes an increment in stress.

Two arbitrary points A (0.05, 0.45) and B (0.05, 0.5) are selected to investigate the wave propagation. Fig. 6 shows the comparison of σ_x , σ_y , and σ_{von} at different times. At $t = 35 \mu s$ only the wave in the x-direction is crossed from point A, so the value of σ_x is equal to the incident wave and σ_y that is made by Poisson's ratio effects. But point B is affected by the wave in x and y directions, so history of stress shows that σ_x and σ_y are equal to the summation of stress wave and the effects of Poisson's ratio on them. The von Mises stress is also calculated at this point to show the behavior of stress in different directions.

The compression of numerical and analytical stresses in Fig. 6 shows that they have acceptable adaptation.

Now for FGM media, initially, the displacement, stresses, and von Mises stress diagrams are plotted and analyzed for three different times and in 5 different states. Then, 4 points are considered on the four sides of the body, and the analysis is done on them. The distributions of displacements component $u(x, y)$ and $v(x, y)$ are plotted in Figs. 7 and 8. The displacements $u(x, y)$ are shown in the five states and at three different times.

The diagrams show that the axial displacement in the third state has the highest value and, conversely, state 2 has the lowest value. But the apparent motion of the particles in each of the five states is almost the same. Also, by comparing all states, in the fifth state, the wave has reached the end of the FG media earlier and has returned. In all states, the u-displacement is positive.

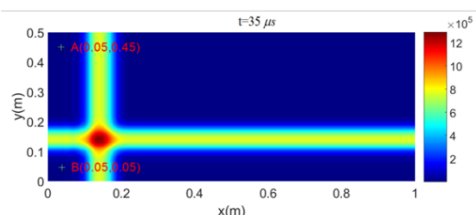


Fig. 5. The von Mises stress distribution in an isotropic media.

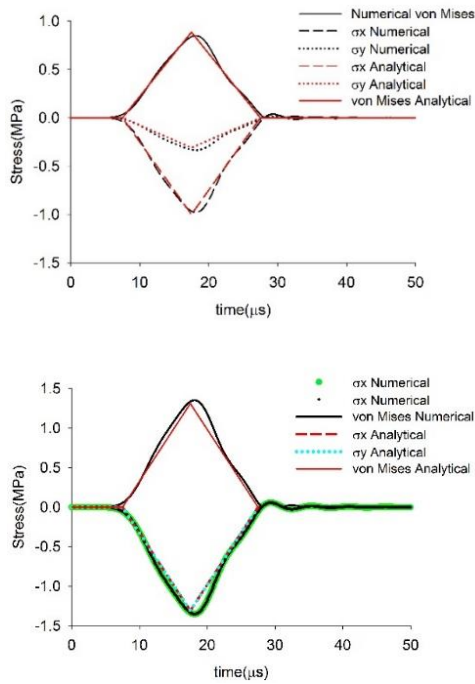


Fig. 6. Analytical and numerical wave propagation compression in an isotropic media.

Relatively, vertical displacement $v(x, y)$ values in this study are larger than the axial displacement. In Fig. 8 vertical displacements are plotted for five states and in three times. As it is known and in all cases, for the time being, the wave has reached the end of the FG media and reflected. It is observed that in state 5, particle velocity is faster than the other states, and conversely, the lowest velocity of particle displacement is related to state 4.

The distributions of the von Mises Stress (σ_v) are plotted in Fig. 9 for the five different states at 35, 65, and 95 μs, respectively.

As seen in these figures, the maximum of von misses stress occurs in the interaction of horizontal and vertical waves. The path of the maximum stress is different in states 1-5. It's depended on the Impedance of material distribution. Moreover, when the impedance changes, the transient and reflected wave changes and this problem complicate the prediction of stress wave especially after reflection of the wave from the edges of the plane. The maximum stress happens in state 1 and in time 65 μs and the level of stress in state 3 is less than in other states.

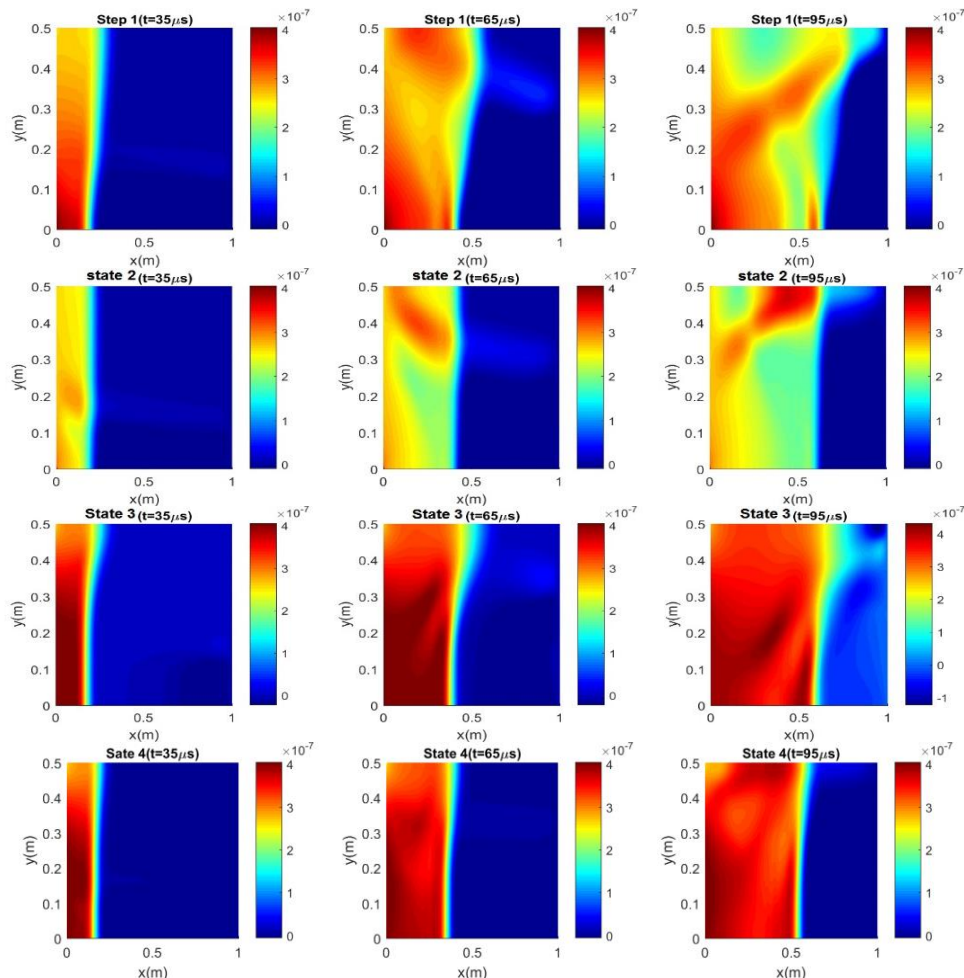


Fig. 7. Distribution of the axial displacement $u(x, y)$ for the five states in 35, 65, and 95 μs.

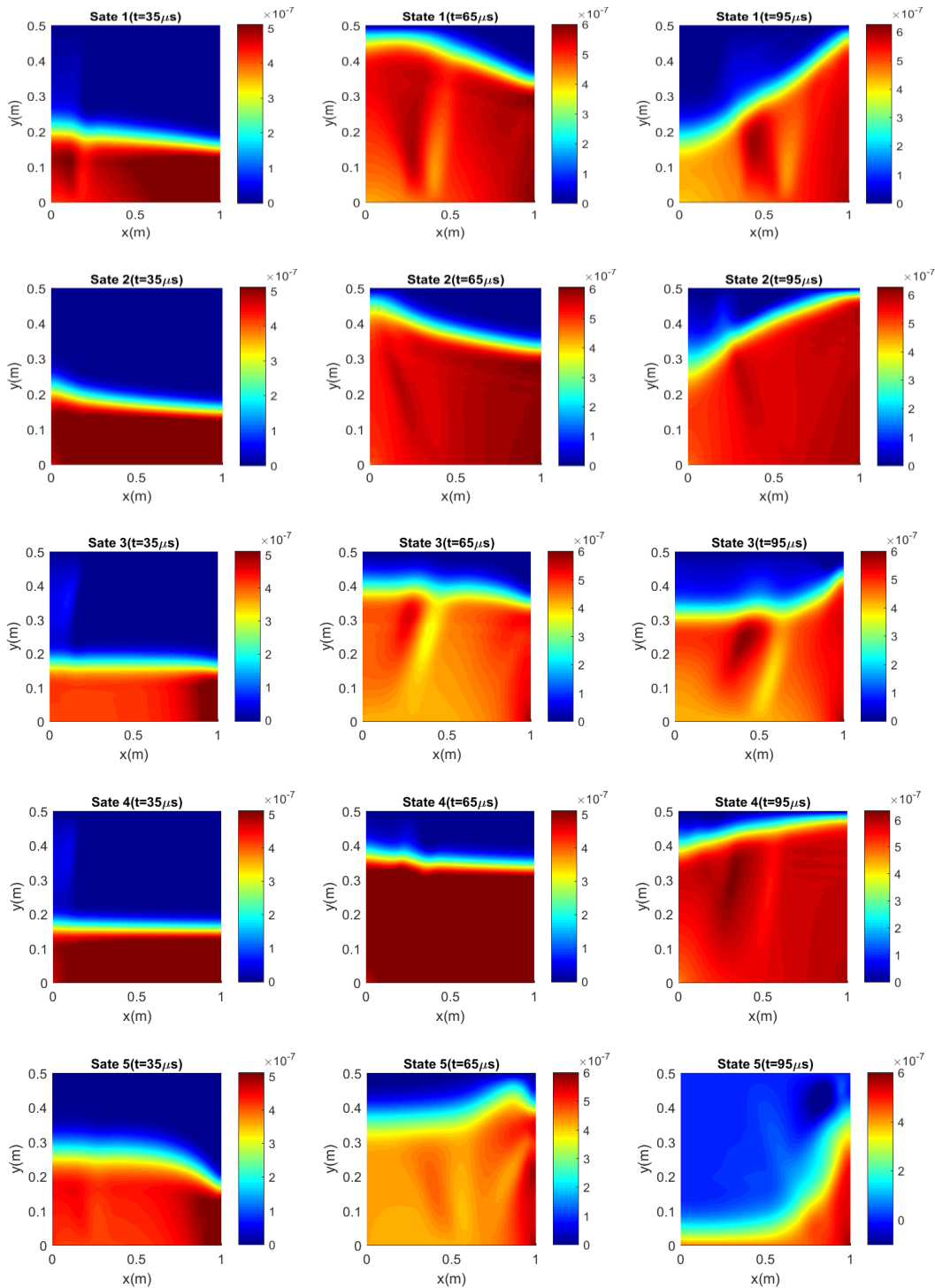


Fig. 8. Distribution of the vertical displacement $v(x, y)$ for the five states in 35, 65, and 95 μs .

As seen in these figures, the maximum of von-mises stress occurs in the interaction of horizontal and vertical waves. The path of the maximum stress is different in states 1-5. It's depended on the Impedance of material distribution. Moreover, when the impedance changes, the transient and reflected wave

changes and this problem complicate the prediction of stress wave especially after reflection of the wave from the edges of the plane. The maximum stress happens in state 1 and in time 65 μs . and the level of stress in state 3 is less than in other states.

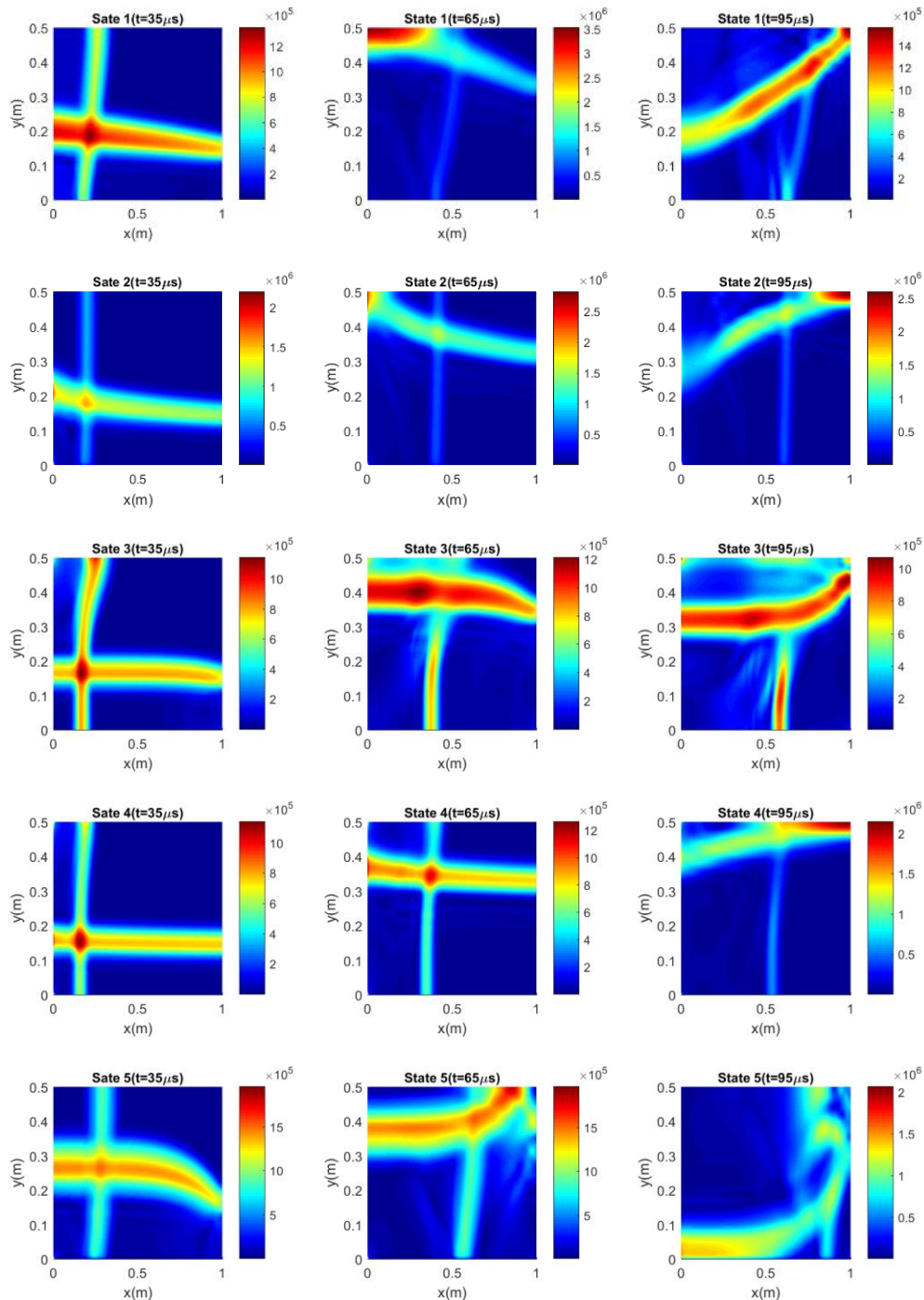


Fig. 9. Distribution of the von Mises stress (σ_v) for the five states in 35, 65, and 95 microseconds.

In Fig. 10 and Fig. 11 the time histories of u and v displacement components are computed at evaluation points A (0.2, 0.4), B (0.8, 0.4), C (0.2, 0.1) and D (0.8, 0.1).

In Fig. 10 the time histories of displacement in x -direction were evaluated for 5 states at points A, B, C, and D. Once the load is applied on the left surface of the FG media, the wave will reach points A and C firstly. With the comparison of time in different states, it is observed that at the instant of 3 microseconds in state 5, the wave reaches point A. then, after a short time, at states 1, 2, 3, and 4 wave reaches this point (point A). As

it is known, the maximum displacement at point A is related to state 3 and state 4. Also on average, the minimum level of change in this interval for this point is related to state 2.

In Fig. 11 the time histories of displacement in y -direction were evaluated for 5 states at points A, B, C, and D. Once the load is applied on the left surface of the FG media, the wave will reach points A and C firstly. With the comparison of time in different states, it is observed that at the instant of 3 microseconds in state 5, the wave reaches point A. then, after a short time, at states 1, 2, 3, and 4 wave reaches this point (point A). As

it is known, the maximum displacement at point A is related to state 3 and state 4. Also on average, the minimum level of change in this interval for this point is related to state 2.

After point A, we arrive to point B, as shown in the diagram. The wave first reaches point B at 4.1 microseconds in state 5, after that at 5.78 microseconds, and in state 1, the wave goes to point B. And finally, at 6.2 microseconds, waves have reached point B in states 2 and 4. It is noteworthy that in state 4, up to 12 microseconds, the variations in the displacement-time graph are very small, but after a 12 microsecond, a significant slope has been achieved.

An optional point C is assumed at the bottom and left of the FG media. In this diagram, wave at first in state 5 arrived to point C and then in other states arrived at this point. It is noteworthy that although the wave amplitude is different in these five states, but it can be said that the wave in all states has the same behavior at point C. the maximum value of the axial displacement in point C is observed at state 3.

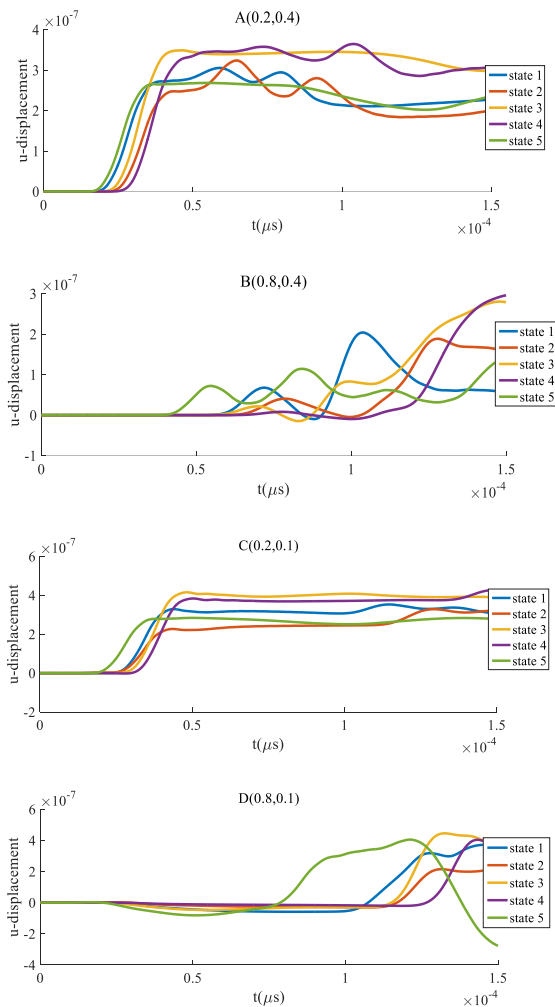


Fig. 10. Time histories of axial displacement at A (0.2, 0.4), B (0.8, 0.4), C (0.2, 0.1), D (0.8, 0.1).

Point D is considered at the end of the functionally graded media to show changes in the axial displacement of particles in this area. In all states, except for the 5th state, after 10 microseconds, the wave has reached point D. At $t = 14 \mu s$, the vertical displacement value has changed from positive to negative.

Figure 11 shows the variations of the v displacement at 15 microseconds at four points (A, B, C, and D) for the 5 states of FG media.

In point A, in all five states, the wave arrived at $t = 3 \mu s$. The vertical displacement at $t = 7.2 \mu s$ has reached its highest value in state 4. Also, the smallest variation in vertical displacement at point A is relative to state 5.

In point B, the vertical displacement in the positive direction becomes maximal at $t = 7.4 \mu s$ in states 2 and 4. Also, the minimum peak occurred in state 5.

The third diagram in Fig. 10 is related to the vertical displacement of point C. in all states, between 0.8 to 1.2 μs , the wave reached point C. According to the diagram and in this period of time, it is shown that the minimum variation in this point occurred at states 4.

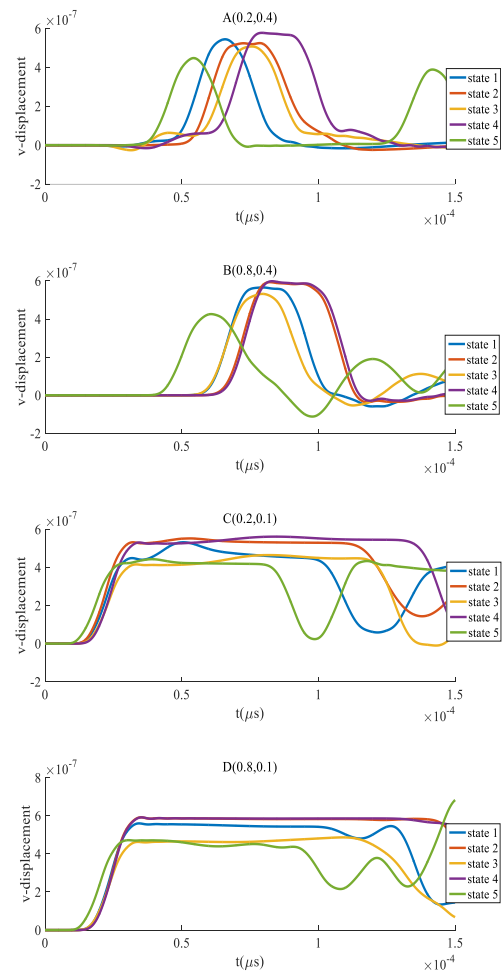


Fig. 11. Time histories of vertical displacement at A (0.2, 0.4), B (0.8, 0.4), C (0.2, 0.1), D (0.8, 0.1).

In point D, although the first excitement occurred at $t = 1.4 \mu\text{s}$, with the passage of time, changes of the vertical displacement at this point are close to zero in states 2 and 4. In state 5, the difference in the peak normal displacement levels are more discernible in comparison with the other states.

Figure 12 shows the variations of σ_{xx} , σ_{yy} and σ_v stress components at point A in the period of $t = 15 \mu\text{s}$ for five states of functionally graded media. Point A has been selected near the loading zone.

At first, σ_{xx} becomes maximal at $t = 3 \mu\text{s}$ in state 5 and over time, amplitudes have decreased, after that, states 1, 3, 2, and 4 reach their maximum point, respectively. At point A with comparison σ_{xx} and σ_{yy} , diagrams, it is known that the σ_{yy} values in this case are higher than the σ_{xx} .

Also, in all states, the first peak of the σ_{yy} , stress occurred with a longer time delay than the σ_{xx} . In the σ_{xx} , diagram, the maximum value is related to state 5, but this value in σ_{yy} , diagram belongs to state 1. The third diagram in Fig. 11 is regarding to the von Mises stress that in this research is shown with a σ_v . In σ_v , the diagram, it is observed that after a small initial peak, there are two large peaks for all the states that the difference between them is almost 0.5 MPa. Contrary to the two preceding diagrams, in Fig. 12, von Mises stress values are obtained positively. Fig. 13 shows distributions of the σ_{xx} , σ_{yy} , and σ_v at point B in five states for FG media.

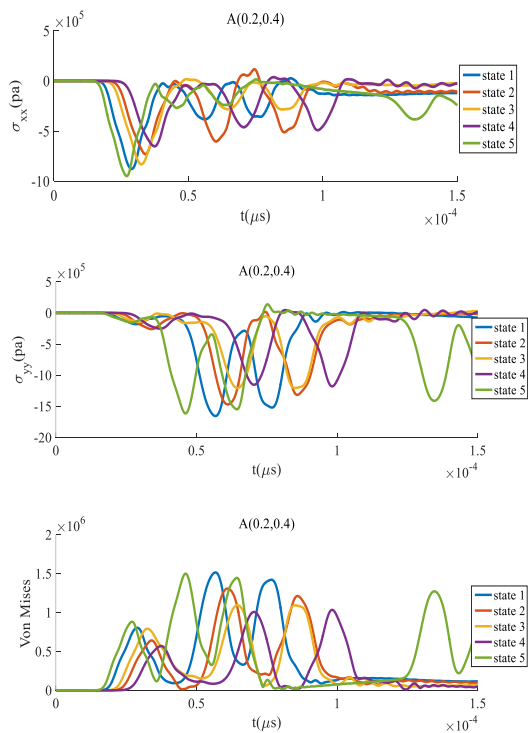


Fig 12. Time histories of σ_{xx} , σ_{yy} , and σ_v stress components at A (0.2, 0.4).

Among the selected points for analysis, the furthest point where the wave reaches is point B. at the end of functionally graded media, point B and in the σ_{xx} diagram, at first because the highest amount of compression is taken by ceramics, so the stress value was taken the amount in state 5. In this diagram, the maximum value of σ_{xx} is related to state 1 at $t = 9.6 \mu\text{s}$.

In the σ_{yy} diagram, accurately to the chart becomes clear that the stress wave of its first peak has experienced at 5.1 microseconds. The maximum value of stress variation in state 2 occurs at 10.8 microseconds. Also, it is noteworthy that in states 2 and 4, due to the compression of the metal, the stress wave in these states with longer intervals reaches point B.

The last diagram in this figure belongs to the von Mises stress (σ_v) at point B. The following information is available from the σ_v diagram: The maximum stress value related to state 5 at $t = 6.8 \mu\text{s}$ first peaks of von Mises stress at point B in states 1, 3 and 2, 4 was occurred between 6.5 to 7.5 microsecond and then after the second peak, the amplitude of σ_v stress is severely reduced. By comparison the σ_{xx} , σ_{yy} and σ_v diagram, it becomes clear that the maximum value of stress in point B occurred in the von Mises diagram.

The time histories of stress components at point C were plotted in Fig. 14.

It is obvious that the wave has reached point C earlier than point A, although two points are located on a radius. It can be seen that the first peak of von Mises has larger value in point C, however generally the maximum value of this stress is larger in point A.

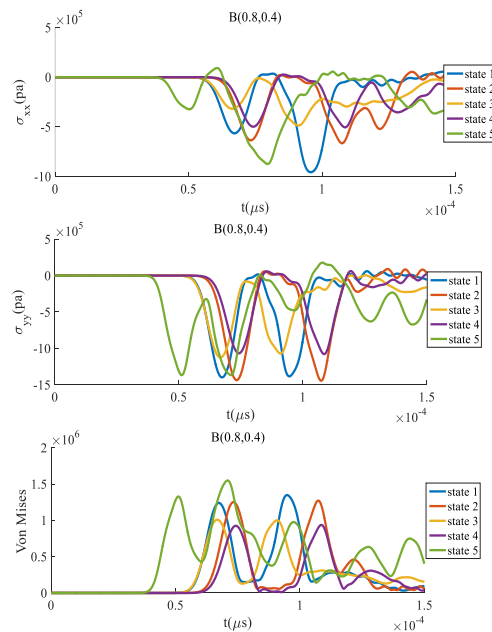


Fig 13. Time histories of σ_{xx} , σ_{yy} , and σ_v stress components at B (0.8, 0.4).

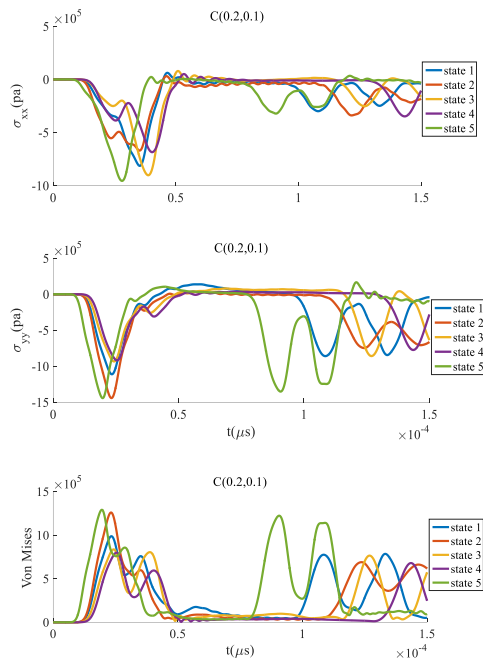


Fig. 14. Time histories of σ_{xx} , σ_{yy} and σ_v stress component at C (0.2, 0.1)

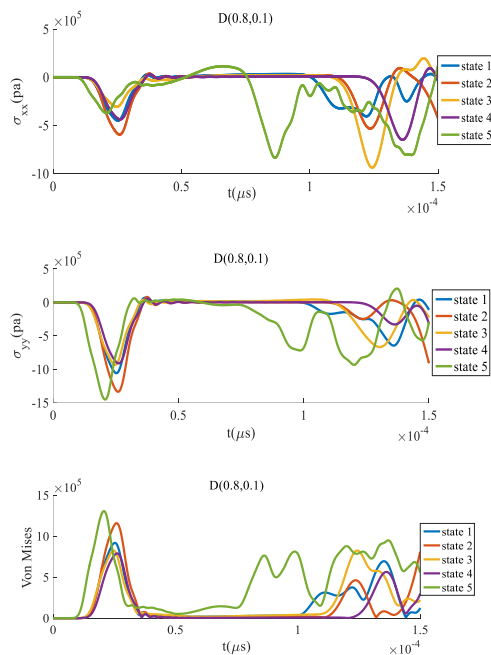


Fig. 15. Time histories of σ_{xx} , σ_{yy} , and σ_v stress components at D (0.8, 0.1).

The time histories of stress components σ_{xx} , σ_{yy} , and σ_v at point D for five states were plotted in Fig. 15.

In this figure, components of stress at point D, the last point assumed in the FG media, are plotted. In this research, points B and D are located on a radius. By comparing Fig. 12 with Fig. 14 it can be seen that the stress wave initially reaches point D and is reached to point B with a time delay, the reason for this is that point D is closer than point

B to the loading. Like previous steps in the σ_{xx} , σ_{yy} , and σ_v diagram, the stress wave was initially reached to point D in state 5. In Fig. 15. The maximum value of stress is related to σ_v .

In this study, it was observed that when the numerical value n_y is greater than n_x ($n_y > n_x$), the volume fraction of metal will be higher than ceramic. Due to the fact that metal has a higher ability to withstand mechanical stresses than ceramic, therefore, according to the type of distribution and application of external force on the body, the volume fraction of the metal should be more dominant in the direction in which the external force is applied and if the material is exposed to heat, the volume fraction of the ceramic should be considered in order to increase the temperature. According to the values and figures of stress obtained, out of 5 states that were analyzed, In state 4, the power of the volume fraction in the y-direction (n_y) is more than in the x-direction (n_x), so we will have the highest volume fraction of the metal in this case, and according to the analysis, it has shown the highest resistance to the applied force. In state 5, because ($n_y < n_x$), so the highest volume fraction of the ceramic is assigned to this case and the most stress on the body is recorded in this state. Also, it was observed that in state 5, the wave has reached the end of the material earlier and the slowest case of wave motion is related to state 4.

4. Conclusions

This paper investigates 2D functionally graded media composed of Ti6Al4V, Al 1100, SiC, and Al₂O₃ Stress wave propagation in 2 directions. The results show when the composition of the material is ceramic-rich or metal-rich, the changes in stress and displacement distribution are quite noticeable. Moreover, the effects of Al 1100 and Al₂O₃ richness are more than Ti-6Al-4V and SiC respectively. Accordingly, the maximum values of displacements and minimum values of stresses in different investigated points correspond to the fourth state namely $V_{m2} > V_{m1} > V_{c2} > V_{c1}$. On the other hand, It was observed that as the material composition is changed from metal-rich to ceramic-rich namely $V_{m2} < V_{m1} < V_{c2} < V_{c1}$, the σ_{xx} , σ_{yy} , and σ_{von} increase in wave propagation direction whereas the displacement levels decrease. In summary, impedance changes and material composition variation had noticeable effects on wave propagation of the functionally graded media.

References

[1] Koizumi, M., 1993. The concept of FGM, *ceramic transaction, functionally graded materials*. 34, pp.3-10

- [2] Vijay, S., and Rao C. S., 2020. Dry slide wear behavior of 601AC/B4C Selective layered functionally graded material with particulate Ni-P coating. *Materials Research Express*, 6(12), pp.1265g7.
- [3] Meng, W., Zhang, W., Zhang, W., Yin, X., Guo, L. and Cui, B., 2019. Additive fabrication of 316L/Inconel625/Ti6Al4V functionally graded materials by laser synchronous preheating. *The International Journal of Advanced Manufacturing Technology*, 104(5-8), pp.2525-2538.
- [4] Fereidoon, A., Mohyeddin, A., Sheikhi, M. and Rahmani, H., 2012. Bending analysis of functionally graded annular sector plates by extended Kantorovich method. *Composites Part B: Engineering*, 43(5), pp.2172-2179.
- [5] Salehi Kolahi, M.R., Karamooz, M. and Rahmani, H., 2020. Elastic analysis of Shrink-fitted Thick FGM Cylinders Based on Linear Plane Elasticity Theory. *Mechanics of Advanced Composite Structures*, 7(1), pp.121-127.
- [6] Kolsky, H., 1963. *Stress waves in solids* (Vol. 1098). Courier Corporation.
- [7] Graff, K.F., 2012. *Wave motion in elastic solids*. Courier Corporation.
- [8] Achenbach, J., 2012. *Wave propagation in elastic solids*. Elsevier.
- [9] Wang, L., 2011. *Foundations of stress waves*. Elsevier.
- [10] Mehrkash, M., Azhari, M. and Mirdamadi, H.R., 2014. Reliability assessment of different plate theories for elastic wave propagation analysis in functionally graded plates. *Ultrasonics*, 54(1), pp.106-120.
- [11] Alterman, Z. and Karal Jr, F.C., 1970. Propagation of elastic waves in a semi-infinite cylindrical rod using finite difference methods. *Journal of Sound and Vibration*, 13(2), pp.115-119.
- [12] Chiu, T.C. and Erdogan, F., 1999. One-dimensional wave propagation in a functionally graded elastic medium. *Journal of Sound and Vibration*, 222(3), pp.453-487.
- [13] Bruck, H.A., 2000. A one-dimensional model for designing functionally graded materials to manage stress waves. *International Journal of Solids and Structures*, 37(44), pp.6383-6395.
- [14] Han, X., Xu, D. and Liu, G.R., 2002. Transient responses in a functionally graded cylindrical shell to a point load. *Journal of Sound and Vibration*, 251(5), pp.783-805.
- [15] Tadi, M., 2004. Finite difference methods for elastic wave propagation in layered media. *Journal of Computational Acoustics*, 12(02), pp.257-276.
- [16] Asemi, K., Akhlaghi, M. and Salehi, M., 2012. Dynamic analysis of thick short length FGM cylinders. *Meccanica*, 47(6), pp.1441-1453.
- [17] Cao, X., Jin, F., Jeon, I. and Lu, T.J., 2009. Propagation of Love waves in a functionally graded piezoelectric material (FGPM) layered composite system. *International Journal of Solids and Structures*, 46(22-23), pp.4123-4132.
- [18] Cao, X., Jin, F. and Jeon, I., 2011. Calculation of propagation properties of Lamb waves in a functionally graded material (FGM) plate by power series technique. *NDT & E International*, 44(1), pp.84-92.
- [19] Hedayatrasa, S., Bui, T.Q., Zhang, C. and Lim, C.W., 2014. Numerical modeling of wave propagation in functionally graded materials using time-domain spectral Chebyshev elements. *Journal of Computational Physics*, 258, pp.381-404.
- [20] Golub, M.V., Fomenko, S.I., Bui, T.Q., Zhang, C. and Wang, Y.S., 2012. Transmission and band gaps of elastic SH waves in functionally graded periodic laminates. *International Journal of Solids and Structures*, 49(2), pp.344-354.
- [21] Dao, D.K., Ngo, V., Phan, H., Pham, C.V., Lee, J. and Bui, T.Q., 2020. Rayleigh wave motions in an orthotropic half-space under time-harmonic loadings: A theoretical study. *Applied Mathematical Modelling*.
- [22] Shariyat, M., Lavasani, S.M.H. and Khaghani, M., 2010. Nonlinear transient thermal stress and elastic wave propagation analyses of thick temperature-dependent FGM cylinders, using a second-order point-collocation method. *Applied Mathematical Modelling*, 34(4), pp.898-918.
- [23] Shariyat, M. and Nikkhah, M., 2009. An exact elastodynamic solution for functionally graded thick-walled cylinders subjected to dynamic pressures. *Iranian Journal Of Mechanical Engineering*, 10(1), pp.55-76.
- [24] Hosseini, S.M. and Abolbashari, M.H., 2010. General analytical solution for elastic radial wave propagation and dynamic analysis of functionally graded thick hollow cylinders subjected to impact loading. *Acta Mechanica*, 212(1-2), pp.1-19.
- [25] Aksoy, H.G. and Şenocak, E., 2009. Wave propagation in functionally graded and layered materials. *Finite elements in analysis and design*, 45(12), pp.876-891.
- [26] Dorduncu, M., Apalak, M.K. and Cherukuri, H.P., 2015. Elastic wave propagation in functionally graded circular cylinders. *Composites Part B: Engineering*, 73, pp.35-48.
- [27] Cherukuri, H.P. and Shawki, T.G., 1996. A finite-difference scheme for elastic wave propagation in a circular disk. *The Journal of*

- the Acoustical Society of America*, 100(4), pp.2139-2155.
- [28] Asgari, M., 2016. Material optimization of functionally graded heterogeneous cylinder for wave propagation. *Journal of Composite Materials*, 50(25), pp.3525-3528.
- [29] Bednarik, M., Cervenka, M., Groby, J.P. and Lotton, P., 2018. One-dimensional propagation of longitudinal elastic waves through functionally graded materials. *International Journal of Solids and Structures*, 146, pp.43-54.
- [30] Yang, Y. and Liu, Y., 2020. A new boundary element method for modeling wave propagation in functionally graded materials. *European Journal of Mechanics-A/Solids*, 80, p.103897.
- [31] Asgari, M. and Akhlaghi, M., 2009. Transient heat conduction in two-dimensional functionally graded hollow cylinder with finite length. *Heat and mass transfer*, 45(11), pp.1383-1392.
- [32] Bin, W., Jiangong, Y. and Cunfu, H., 2008. Wave propagation in non-homogeneous magneto-electro-elastic plates. *Journal of Sound and Vibration*, 317(1-2), pp.250-264.
- [33] Vollmann, J., Profunser, D.M., Bryner, J. and Dual, J., 2006. Elastodynamic wave propagation in graded materials: simulations, experiments, phenomena, and applications. *Ultrasonics*, 44, pp.e1215-e1221.
- [34] Asgari, M. and Akhlaghi, M., 2011. Natural frequency analysis of 2D-FGM thick hollow cylinder based on three-dimensional elasticity equations. *European Journal of Mechanics-A/Solids*, 30(2), pp.72-81.
- [35] Amiri, A., Rahmani, H. and Ahmadi Balootaki, M., 2020. Torsional wave propagation in 1D and two dimensional functionally graded rod. *Journal of Computational Applied Mechanics*, 51(1), pp.1-21.
- [36] Otieno, O.R., Manyonge, A., Maurice, O. and Daniel, O., 2015. Finite Difference Analysis of 2-Dimensional Acoustic Wave with a Signal Function. *International Journal of Multidisciplinary Sciences and Engineering*, 6(10).